IEEE Transactions on Quantum Engineering

Received 11 September 2024; revised 7 February 2025; accepted 12 February 2025; date of publication 17 February 2025; date of current version 13 March 2025.

Digital Object Identifier 10.1109/TQE.2025.3542484

Qubit Rate Modulation-Based Time Synchronization Mechanism for Multinode Quantum Networks

MARC JOFRE

Department of Network Engineering, Universitat Politècnica de Catalunya, 08860 Castelldefels, Spain

Corresponding author: Marc Jofre (e-mail: marc.jofre@upc.edu).

This work was supported in part by the Agencia Estatal de Investigación (Spain) under Grant PID2022-137329OB-C41, Grant PID2022-136869NB-C31 (MCIN/AEI/10.13039/501100011033/FEDER, UE), Grant CNS2024-154600, and Grant PDC2022-133091-I00, in part by the Catalan Government University and Research Aid Management Agency (AGAUR) with Research Group under Grant 2021 SGR 01046, and in part by the Technical University of Catalonia (UPC) under Grant ALECTORS 2024.

ABSTRACT The combination of quantum and telecommunication networks enables to revolutionize the way information is used, offering unparalleled capabilities and making it an ideal choice for many critical applications. In this sense, quantum protocols generally have a unique requirement to have strict time synchronization in order to operate, which generally consume quantum resources of part of the exchanged qubits. Accordingly, work demonstrates and characterizes a temporal alignment mechanism for quantum networks based on frequency testing, allowing to preserve the quantum state of qubits. The time synchronization correction achieved is within 100 ns working at 5 MHz with temporal and relative frequency offsets commonly acquired in quantum links using conventional hardware clocks with temporal stability in the range of 10^{-8} and 200-ns jitter.

INDEX TERMS Communications, distributed clocks, links, mechanisms, network interoperability, projective measurements, protocols, quantum networks (QNs), qubits, synchronization.

I. INTRODUCTION

Quantum networks (QNs) are necessary for the applicability and distribution of quantum resources. This exchange of quantum states over distances, generally requiring the support of classical communications, will enable new capabilities to communication systems [1]. The proper use of quantum information makes feasible solutions to use the combined concurrent and nonseparable calculation capabilities of quantum operations in distributed tasks, such as for leader election, Byzantine agreement, coin flipping, and distributed references. These capabilities enable a plethora of applications, including distributed computing [2], [3], enhanced and distributed sensing [4], [5], secure communications [6], [7], [8], entropy generators [9], [10], [11], detection and ranging [12], [13], and clock synchronization [14], among others [1], [15].

These applications will depend on communication between quantum systems over quantum local area networks (QLANs). Furthermore, when advanced quantum devices become available, such as routers, queue systems, bridges, and other networking devices [16], [17], [18], [19], this will expand to other types of network extensions such as metropolitan area networks, wide-area networks, and the future quantum internet [20], [21].

In particular, time synchronization of all nodes in the network is important in quantum protocols, such as in entanglement swapping as well as for the detection of qubits. Furthermore, time stamping of detected qubits in discrete variable protocols is very efficient resourcewise [22]. In spite of the strict temporal synchronization for the detected qubits, future quantum memories will be able to accommodate for some time requirements, up to a certain time span [23]. Nevertheless, QNs will still require tight qubit time synchronization primitives to reach the fidelities of quantum operations, scalability with multinodes, and overall efficiency of networks.

In this direction, quantum protocols are in need of time synchronization mechanisms, which reliably account for the intrinsic specifics of communicating with qubits, for example, individually identifying sparsely distributed detected qubits, coincidences, or allowing them to interfere in order

to use their quantum allocated information. In this regard, early systems using point-to-point transmission of qubits are synchronized individually by allocating a classical channel solely for synchronization purposes (e.g., clock distribution) or using optical references. However, more recent works have already started to demonstrate capabilities to time-synchronize QNs (or at least the QLAN part) [24], [25], [26], [27], [28], [29] making use of conventional networking time synchronization protocols [30], [31], [32] at the network system level. The network time protocol (NTP) [30] is one of the most widely used protocols, designed to synchronize clocks of computers over packet-switched variable-latency data networks. The NTP can achieve millisecond accuracy over the Internet and even better performance on local networks. For higher precision, the precision time protocol (PTP) [31], defined by IEEE 1588, is preferred. The PTP is capable of achieving submicrosecond accuracy, making it suitable for applications in industrial automation and telecommunications. An even more precise protocol is White Rabbit [32], an extension of PTP, which achieves synchronization to within a nanosecond.

Aside from the local stability of hardware clocks, even if using very precise systems (e.g., atomic clocks) at each node, networks benefit from absolute time reference. Note that time synchronization is the strictest of the different synchronization possibilities, being the other phase and frequency. Furthermore, in multinode QNs, it is convenient to reduce the need to rely on adaptive synchronization algorithms based on the qubits of the running quantum protocol, since they generally entail destroying or revealing the quantum state with nonprojective measurements. Furthermore, this would make these qubits useless for quantum protocols, as many would have to be exchanged as classical information for post-compute synchronization.

This work describes a temporal synchronization mechanism for QNs that does not consume the exchanged quantum information. This mechanism is based on frequency testing with qubit signals with the support of a time-synchronized Telecom network. The mechanism allows one to extract the temporal and relative frequency offsets for each quantum link connecting two nodes in the QN, conveniently updating the synchronization parameters in a periodic way.

The objectives of this work are to: 1) derive a system of equations to characterize the temporal synchronization of quantum links and propose a mechanism to derive the relevant parameters; 2) assemble an experimental system to implement the mechanism; and 3) provide measurements and discuss the results achieved with regard to common quantum protocols.

The rest of this article is organized as follows. Section II describes the theoretical model for time synchronization and the procedure to implement the proposed mechanism. An implementation of the necessary components to assemble a time-synchronized QN is provided in Section III. Measurement and analysis are discussed with results in Sections IV and V, respectively. Finally, Section VI concludes this article.

II. THEORETICAL DESCRIPTION

For quantum applications, it is of interest to distribute quantum resources along a network, which entails transmitting qubits to other remote nodes. Nevertheless, quantum information is physically produced locally, and consequently, qubits have to be sent to another remote node connected to the network. At the same time, this remote node is most commonly located at a distance that differs from the distances of other nodes, or the equivalent transmission distance might change due to network configuration. Hence, if this is not accounted for, it results in different time of arrival of qubits to the node where it is desired to utilize the qubits for exploiting quantum resources.

In this context, the system space part of a QN entails the operating system responsible for running software instructions on the nodes related to control and management, while at the real-time space of a QN, the hard-coded hardware instructions run at the chip level. Accordingly, in the real-time space, where the quantum signals are processed, time synchronization can be disciplined to the system space clock controlled by the operating system in accordance with network time synchronization protocols.

On the one hand, the time of arrival of remotely generated qubits to a common node is different for each link and dependent on the distances qubits have to transit. Therefore, it is not practical to handle these temporal offsets, which can be up to milliseconds, solely considering the use of future quantum memories, as a proxy for queue management, mainly because much of this time difference consists of a constant offset that can be compensated. However, the time of generation of qubits is controllable, at least within a picosecond time span related to the spectral bandwidth of the generated qubits [33]. Consequently, the time of generation of the qubit can be triggered at instants within specific allocated time slots (t_s) to match the time of arrival to a common node of qubits of different links.

On the other hand, QNs can be time synchronized at the system level with standard Telecom time synchronization protocols. This is important when accounting for QNs with multiple nodes, rather than only point-to-point communication links. Nevertheless, despite synchronizing the network at system level, it is of utmost importance to align temporally the physical qubits in the real-time part of the QN. Therefore, as shown in this work, the quantum part of the network can be temporally aligned for common quantum protocols with measurements.

In quantum communications, synchronization can rely on the temporal alignment of classical signals with qubit arrival times. Temporal correlations between detection events can provide valuable information for this purpose, as shown in [14]. In this work, a precise mapping of the detection times of incoming qubits to classical signal announcements is employed. Let t_{QB_n} denote the arrival time of a detected

IEEE Transactions on Quantum Engineering

qubit, and let $\theta_{q_{ab_n}}$ represent the timing of the associated classical synchronization signal, where $n \in \mathbb{N}^+$ denotes the time slot number, as further detailed in this section. The root-mean-square (rms) timing jitter σ_t is defined as the standard deviation of the arrival time differences of qubits with respect to the beginning of the respective time slot n as

$$\sigma_t = \sqrt{\mathbb{E}\left[\left(t_{QB_n} - \theta_{q_{ab_n}}\right)^2\right] - \left(\mathbb{E}\left[t_{QB_n} - \theta_{q_{ab_n}}\right]\right)^2} \quad (1)$$

where $\mathbb{E}$ is the expected value operator over multiple detections of qubits. Then, using single-photon detectors with an rms timing jitter σ_t of approximately 140–180 ps, it is ensured that $|\theta_{q_{ab_n}} - t_{QB_n}| \ll T_H$, where T_H is the temporal separation between emitted qubits.

Let the quantum state of the incoming qubit be represented as $|\psi\rangle$. The qubit is typically encoded in a temporal mode defined by a wavepacket $f(t)$, where $f(t)$ is normalized such that $\int_{t_s} |f(t)|^2 = 1$. The detection process projects the qubit state onto a time-bin t_{QB_k} determined by the timing resolution and jitter of the detector. For synchronization, a classical signal is generated at time $\theta_{q_{ab_n}}$, which is derived from the detection event at t_{QB_n}. To ensure that the classical signal correctly maps the timing of the detected qubit, the condition is imposed that the timing uncertainty introduced by the detector jitter δt_{SPAD} satisfies

$$\sum_n \frac{|\theta_{q_{ab_n}} - t_{QB_n}|}{n} = \delta t_{\text{SPAD}} \quad (2)$$

$$\delta t_{\text{SPAD}} \ll T_H. \quad (3)$$

The qubit pulse train, defined as a state of temporally separated wavepackets, can be expressed as $|\Psi\rangle = \sum_n c_n f(t - nT_H)$, where c_n are complex amplitudes and n indexes the qubits in the train. For synchronization, the classical timing signal must preserve the distinguishability of individual qubit wavepackets within the pulse train. This requires that the timing offset $|\theta_{q_{ab_n}} - t_{QB_n}|$ is sufficiently small such that there is a negligible overlap between adjacent wavepackets $f(t - nT_H)$. Thus, the condition $|\theta_{q_{ab_n}} - t_{QB_n}| \ll T_H$ ensures that the classical timing signals maintain a one-to-one correspondence with the qubit arrival times, preserving the integrity of the quantum information encoded in the pulse train. Since this synchronization process relies solely on classical timing information, it does not depend on the quantum state $|\psi\rangle$ of the qubit. This independence enables compatibility with a wide range of quantum communication protocols, including quantum key distribution (QKD), quantum teleportation, and entanglement distribution.

In this sense, a QN with such functionality can be assembled as shown in Fig. 1(a), although, in general, any other QN topology and the number of nodes could also be considered for the proposed mechanism. In particular, the quantum nodes cooperate with the functionalities of the classical network for control and management and also for time synchronization purposes.

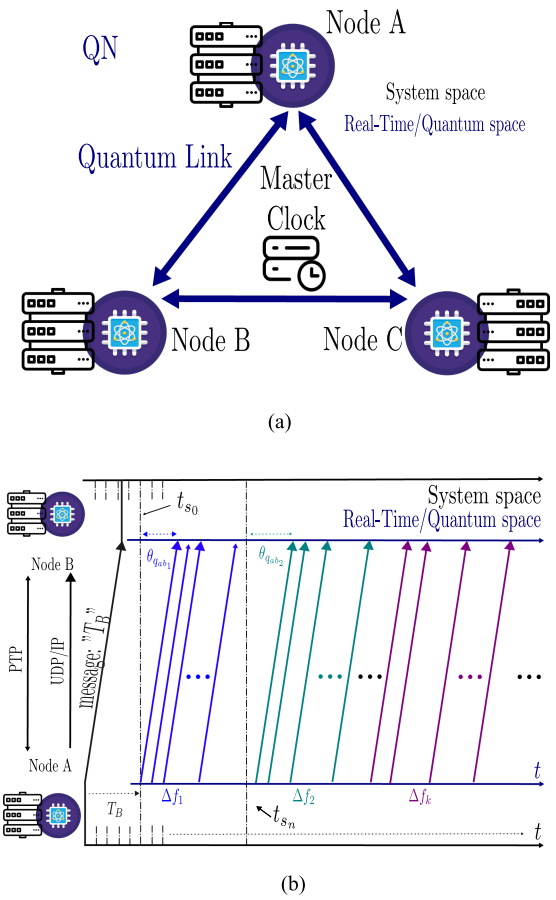

FIGURE 1. (a) Scheme of a QN. (b) Temporal diagram of the qubits sent through the quantum link between nodes A and B when applying the proposed mechanism.

Ideally, the temporal alignment of the real-time space of the network, which includes the quantum part, to the telecommunications synchronized system network is achieved by taking into account the propagation time of the qubits and the relative frequency difference to their respective quantum nodes, as shown in Fig. 1(b). In particular, one of the participating nodes in the communications, e.g., node A, first sends a User Datagram Protocol/Internet Protocol (IP) network message to the other node notifying the system time synchronization barrier T_B, which is a time point 3 s in advance of the actual time, to align themselves to start emitting and receiving qubit signals, respectively. Then, the proposed mechanism in this work executes the procedure to measure the intrinsic time delay in the quantum components as well as relative frequency offsets. In order to accomplish this procedure, partial frequency synchronization is obtained from the system space clock, and it is transferred to the real-time space quantum nodes, while phase and relative frequency offsets are periodically corrected and updated.

In general, the real-time clock offset between nodes A and B is

$$\theta_{q_{ab}} = t_{q_{b_2}} - t_{q_{a_1}} \quad (4)$$

where $t_{q_{a_1}}$ is the trigger time of qubits at node A, and $t_{q_{b_2}}$ is the time of tagging of qubits at node B. In turn, considering triggered qubits accounting for constant and nonconstant network delays, and applying the proposed mechanism to retrieve the synchronization parameters, the offset can be described as

$$\theta_{q_{ab_k}} = (\Delta f_k + \delta f)\, t_{s_n} + \theta'_{q_{ab}} \tag{5}$$

where Δf_k is a selectable frequency between $k \in \mathbb{N}^+$ test requests, δf is the relative frequency offset (the difference in operating frequencies between two nodes), t_{s_n} is the triggering time (precise up-front PTP time slot when qubits are emitted from the transmitter node) of the qubits in their time slot (t_s), $n \in \mathbb{N}^+$ indicates the time slot number, $\theta'_{q_{ab}}$ is the constant phase offset between nodes A and B, and $\theta_{q_{ab_k}}$ is the overall phase offset for the particular iteration k of the mechanism. Note that selectable frequency denotes the capability to dynamically choose the operating frequency of the transmitter at each test request of the mechanism, where test request is each iteration of the synchronization mechanism of this work working with a different selected frequency.

The demonstrated mechanism in this work is depicted in Fig. 2. First, Fig. 2(a) shows three different values of Δf_k, which equivalently produce different effective temporal offsets. Then, Fig. 2(b) shows the emission and detection times (in units of time slots) when the previous values Δf_k are used sequentially together with the presence of an initial offset $\theta'_q = 0.05$, $\delta f = 0.001$ (normalized to the histogram period (T_H), and $l = 15$ qubits per sequence. Finally, in Fig. 2(c), the detected events are represented using a histogram that allows one to graphically visualize the synchronization status of the link and the effects of the applied mechanisms parameters. In particular, in the histogram representation, the effects of θ'_q and δf (as well as Δf_k) arise because the detection times are offset from the center of the histogram. In general, the equivalent offset produced by δf fits in the histogram period T_H because δf is small relative to T_H. Instead, θ'_q is larger than T_H, so only the remaining modulo T_H is visualized (nevertheless, the absolute value of θ'_q is retrieved as explained later).

Furthermore, the mechanism can handle a separation in number of time slots between the different k iterations to have a guard time (D_s) to clearly distinguish different applied Δf_k.

Let us assume that both nodes A and B each have a clock synchronized in time in system space, but at the real-time space, there is a phase $\theta'_{q_{ab}}$ and relative frequency δf difference offsets between them. The mechanism proposed in this work applies a multistep ticking qubit handshake, where Δf_k is varied in a selectable and controlled way, resulting in a measurable phase offset $\theta_{q_{ab_k}}$. Once these parameters have been estimated at the receiver node, these parameters are communicated back to the transmitter node via a classical channel to complete the multistep qubit ticking handshake procedure.

Also, this mechanism preserves the quantum state of the qubits by using only projective measurements of their arrival

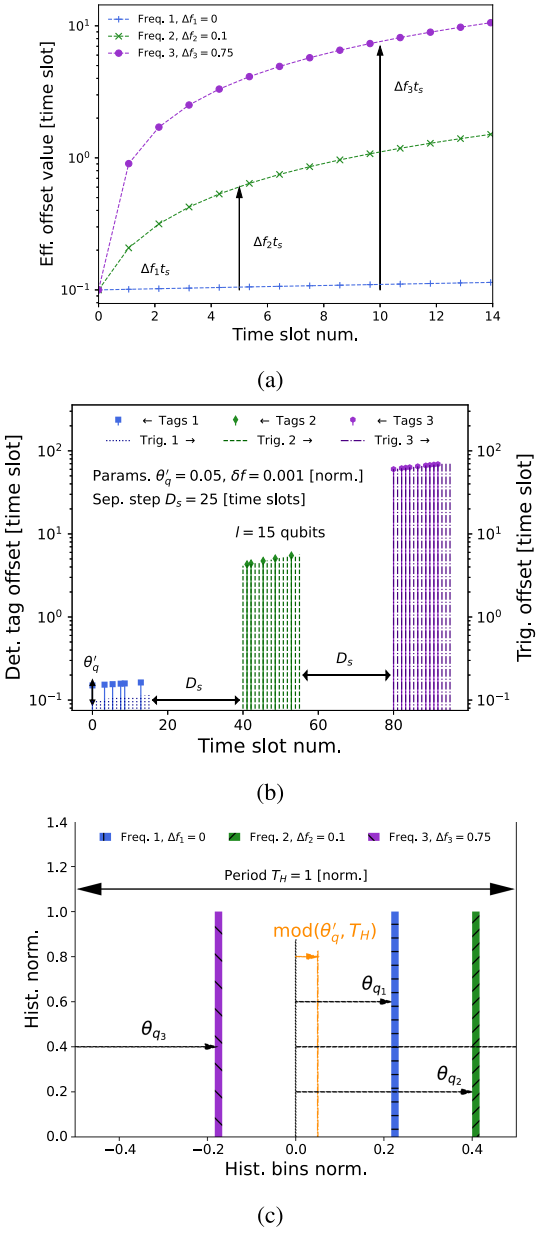

FIGURE 2. Depiction of the mechanism procedure. (a) Temporal offset evolution applying different Δf_k. (b) Time offset of the triggered events and time tags of the detected qubits. (c) Temporal alignment mechanism histogram to retrieve the synchronization parameters.

times. As a result, the quantum information encoded in their wave functions remains intact, without being revealed or collapsed.

Then, by solving the system of linear equations, the unknowns δf and $\theta'_{q_{ab}}$ are retrieved. Consequently, the mechanism can retrieve the phase offset between nodes A and B, as well as the relative frequency offset. Therefore, at least two different frequencies have to be employed to define a system of two equations. However, notice that additional equations can be added to the system of equations in order to account for the deviations of the time instances t_{s_n}. In addition, as a

IEEE Transactions on Quantum Engineering

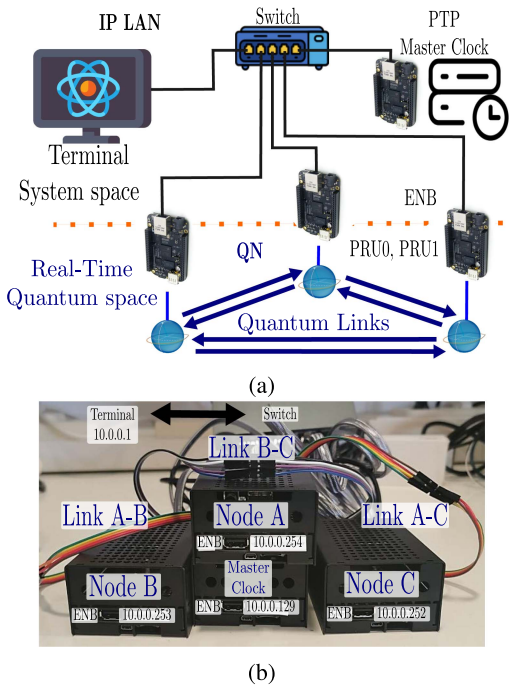

FIGURE 3. (a) Scheme of the assembled experimental system. (b) Picture of the detail of the ENBs nodes and their physical and logical connections.

first approximation for an iterative algorithm for the mechanism, Δf_k can be made generally large compared to δf to rapidly approximate $\theta'_{q_{ab}}$.

Moreover, the specific values of Δf_k can be tuned particularly for the specifics of the quantum link, e.g., values with proportional or nonproportional steps. Finally, the mechanism can be applied periodically to each quantum link to be synchronized, in accordance to the quantum protocols running in parallel on the QN.

Theoretical modeling, as illustrated in Fig. 2, was essential for testing and refining the time synchronization mechanism prior to experimental implementation. It simulated expected time offset behaviors under ideal conditions, providing a benchmark and building confidence in the scheme. However, theoretical models may not fully capture particular experimental nuances, such as interrupt handling times and hardware clock wander.

III. SYSTEM OPERATION

In this section, the experimental temporal synchronization system is described. The system consists of four electronic network boards (ENBs), three of them operating as nodes and an extra one acting as the PTP master clock for the network. All these are connected through a network switch, as shown in Fig. 3(a). Also, six physical link connections are implemented between specific pins of the ENBs to enable the transmission of signals representing qubits. In particular, the physical links are each provided with four effective connections to enable to send equivalent specific states, i.e., quantum state encoding. Furthermore, the nodes are capable of producing l triggered signals with variable temporal relative offset, which translates to operating with an effective frequency Δf_k added to the relative frequency difference δf and phase offset θ'_q.

The nodes are implemented with programmable ENBs with two real-time units each, named programmable real-time units (PRUs). Each node is composed of the system part and the real-time/quantum part. In particular, the real-time part is responsible of emitting and detecting qubits. Furthermore, each node has four connected unidirectional links: two for transmission and two for reception of qubits, the latter allowing to connect all three nodes with six links, as shown in Fig. 3(a).

Also, at each ENB, one of the PRUs periodically (every 100 ms) align in time the real-time space with the system space, except for a constant relative frequency difference. In this way, the real-time part of the nodes follows the network local master PTP clock. Also, the first PRU is used to trigger l qubits at 5 MHz to generate signals to assess time synchronization for each pair of connected nodes. At the same time, the sequence of signals is programmed to randomly drop some triggers to emulate the probabilistic transmission and detection of qubits through a quantum link. Trigger drops are modeled using a Poisson distribution with a mean rate corresponding to a 99% average drop probability. This choice reflects the stochastic nature of qubit losses in quantum communication channels for an effective attenuation of 20 dB. This ensures that the performance of the proposed synchronization mechanism is evaluated under approximate ideal (only losses) quantum channel conditions. The other PRU unit hardware time stamps the detected signals with 5-ns edge detection resolution with a 32-bit counter, and up to 12 channels at a maximum rate of 10 mega counts per second over all channels.

Accordingly, each node has six sets of four emitting/receiving pins, enabling to both control three emitting and attend three receiving links. The latter enables to assemble interconnections between nodes to form networks with different topologies. Note that each group of four pins enables the emission or detection of a qubit, because, in general, a qubit encodes information in one of four possible outcomes, which aligns with typical encoding schemes used in quantum communication protocols. It is important to note that this representation abstracts the quantum nature of the qubit, such as superposition or entanglement, but faithfully represents the qubits detection signals in single-photon detectors. Therefore, this work focuses exclusively on the synchronization mechanism and uses this representation to abstract the complexities of direct quantum state manipulation.

Accordingly, in quantum communication protocols, measuring a single qubit generally requires projections onto two complementary bases, typically the computational basis ($|0\rangle, |1\rangle$) and the diagonal basis ($|+\rangle, |-\rangle$), where $|+\rangle = \frac{1}{\sqrt{2}}(|0\rangle + |1\rangle)$ and $|-\rangle = \frac{1}{\sqrt{2}}(|0\rangle - |1\rangle)$. Each basis corresponds to two distinct outcomes, resulting in four possible

outcomes in total, represented by the measurement operators $M_1 = |0\rangle\langle 0|$, $M_2 = |1\rangle\langle 1|$, $M_3 = |+\rangle\langle +|$, and $M_4 = |-\rangle\langle -|$, which satisfy the completeness relation $M_1 + M_2 + M_3 + M_4 = I$. Using four detectors (four receiving pins in this work), useful information of the qubit states can be resolved, supporting protocols such as QKD and entanglement-based schemes.

Also, the hardware time stamps of the PRU are direct memory access transferred to the system space of each respective node, appropriately converted with 1-ns resolution and 100-ns precision (limited by the residual time error of the ENB) to system space time, referenced to the beginning of the epoch (UNIX convention to 00:00:00 UTC on 1 January 1970).

Specifically, the nodes are implemented with off-the-shelf BeagleBone Black development ENBs [34], as shown in Fig. 3(b). These boards provide 200 MHz at 5-V inputs and output pins directly operated by the real-time chip and clocked with a TCXO 24-MHz board clock. Also, the boards provide several Ethernet network interfaces. One of the Ethernet interfaces implements hardware time stamp capabilities, which enable them to run NTPs such as PTP [35], [36].

In particular, the nodes have been configured to run linuxPTP software implementation according to IEEE Standard 1588 for Linux. The configured PTP Telecom profile G.8275.1 (phase/time profile with timing support) uses end-to-end delay request–response mechanism, Ethernet packet encapsulation, two-step operation, and 100-ns allowed frequency step threshold to achieve rapid and robust time synchronization convergence.

The IP LAN is a switched GigaBit Ethernet with network address 10.0.0.0/24 with UTP-Cat6 cables linked with a layer 2 switch (transparent in terms of IP traffic). In particular, the terminal host has the address 10.0.0.1 in the network and also acts as a router. The nodes have been assigned the upper addresses of the network (10.0.0.252–10.0.0.254), and the PTP master clock has the address 10.0.0.129. The host terminal runs Ubuntu 22.04.4 LTS Linux distribution, and the nodes run on Debian GNU 10 Linux distribution with real-time kernel TI 5.10.

Hence, the master PTP clock runs as an ordinary clock, while time synchronization is achieved throughout the control system network. Then, the time reference of the PRU is disciplined periodically with these time corrections. Correspondingly, the time wander is corrected in each node in the system space and transferred to the real-time space periodically. Nevertheless, it still remains a relative frequency offset between the different nodes in the QN and a phase offset for each quantum link. Therefore, the proposed mechanism of this work is used to adjust these offsets of the real-time quantum part, as demonstrated in the following sections.

IV. EXPERIMENTAL MEASUREMENTS

The proposed temporal synchronization mechanism is experimentally characterized with the system described in Section III. In particular, the focus is on the assessment of the temporal alignment of the different nodes with the emitted/received signals representing qubits. The performance is generally assessed in terms of histogram calculations in the real-time space.

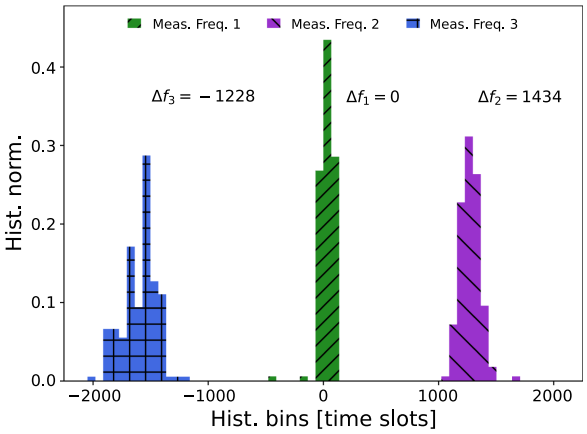

FIGURE 4. Histogram of time detections when performing the synchronization mechanism procedure with three test frequencies.

In the proposed synchronization mechanism, qubit signals are used to estimate propagation delays and relative frequency offsets. This choice ensures that the exact hardware responsible for quantum communication is also used for synchronization, eliminating potential mismatches that could arise from employing classical signals. Therefore, utilizing qubit signals for synchronization ensures a precise alignment with the quantum channel conditions, resulting in improved synchronization accuracy and performance for QN protocols.

First, the synchronization mechanism procedure is depicted in Fig. 4 with three test frequencies Δf_k (with values $\Delta f_0 = 0$, $\Delta f_1 = 1434$, and $\Delta f_2 = -1228$, in time slot units and modulo T_H wrapped), each Δf_k is run six times, and each run $l = 1964$ qubits are detected with $T_H = 4096$. In this regard, the real-time space temporal unit is used in the following results, named as time slots (t_s), which correspond to 5 ns.

Notice that the measured centers of mass for Δf_k different than 0 do not exactly match the imposed displacement. In particular, in Fig. 4, the centers of mass measured for Δf_2 and Δf_3 are 1392 and -1312, respectively. Hence, they suffer from a deviation of 1.03 between the theoretical values and the achieved ones.

Therefore, the three Δf_k are used in order to perform the calculation of the mechanism, as detailed next. First, the three different measured centers of mass, as shown in Fig. 4, are retrieved as H_1, H_2, and H_3, respectively, for Δf_1, Δf_2, and Δf_3. Then, the nominal values of δf and modulus T_H of θ' are computed with (6) and (7) and parameters of interest as

$$\delta f = -(H_0 - \Delta f_0 T_H) \tag{6}$$

$$\mathrm{mod}(\theta'_q, T_H) = \mathrm{median}\,[\mathrm{mod}(TT_i + \delta f T_H, T_H)] \tag{7}$$

IEEE Transactions on Quantum Engineering

TABLE 1. Performance of the Clocks and Processes of the Three Nodes

Node	A	B	C	Average
Clock	Offset error / Jitter std. [ns]			
System	+10 / 30	−12 / 16	+9 / 44	10 / 30
Hardware	+112.5 / 188.3	−91.6 / 205.2	+98.3 / 208.6	100.8 / 200.7
Process	Offset error / Jitter std. [μs]			
Interrupt	4.7 / 2.8	3.8 / 4.1	4.6 / 1.7	4.3 / 2.8
Synchronization wander	1.2 / 0.6	−2.5 / 0.4	0.9 / 0.7	1.5 / 0.5

$$\xi_k = \begin{cases} 1.0, & \text{if } k = 1 \\ \frac{\Delta f_k - \Delta f_0}{H_k - H_0}, & \text{if } k = [2, 3] \end{cases} \tag{8}$$

$$\delta f' = \begin{cases} \xi_1 \delta f, & \text{if } \delta f \geq 0 \\ \xi_2 \delta f, & \text{if } \delta f < 0 \end{cases} \tag{9}$$

where ξ_k are adjustment coefficients multiplied to δf to fine adjust the latter when applying the correction in the real-time space PRU with $\delta f'$, and θ'_q modulo T_H with median averaging all the corrected ($\delta f T_H$) time tagged detected events (TT_i) of the $k = 0$ iteration.

In this direction, measurements of the specific time accuracy for different ENBs acting as nodes are shown in Table 1. The values are shown for the system clock and real-time clock with 500 measurements for each item. These values are the time offset and jitter (standard deviation) with respect to the master PTP clock. In particular, the real-time clock is only composed of the hardware clock time characteristics, when appropriately avoiding the impact of the following running processes. The first process is the interrupts (trigger signal between system space and real-time space) to directly perform absolute time synchronization updates in the ENBs. Rather, the time synchronization error is relatively tracked periodically (querying the real-time clock counter every 100 ms), and it is software corrected in system space. The second process is the overall synchronization wander due to the real-time hardware clock randomly drifting over time (considered 1 s), which is also tracked and software corrected at system space. Then, the achieved average error synchronization value in the real-time space is approximately 100 ns with 200-ns jitter. Notice that the values in the system space are generally better and, therefore, do not limit the performance of the mechanism working in the real-time space.

The system time measurements in Table 1 were obtained with the information logs generated by the phc2sys linuxPTP daemon for each ENB, while the interrupt measurements were characterized with system clock measurements in the develop drivers. Finally, the hardware clock of the real-time characterization was performed using the trigger signals generated from the ENBs and measured using a time tagging unit with resolution of picoseconds (Time tagger 20, Swabian Instruments [37]).

On the one hand, the three different test frequencies Δf_k are differentiated in the measured histogram at one of the detection nodes, as shown in Fig. 4. On the other hand, the histogram analysis shows the temporal spreading due to the applied Δf_k, but still allows computing the center of each

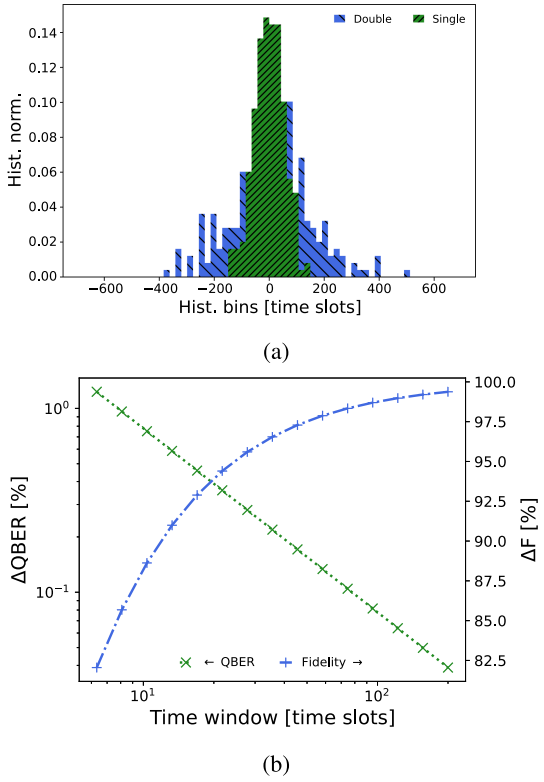

FIGURE 5. Synchronization performance results for PTP disciplined nodes. (a) Detection time difference for single and double detections. (b) Impact of the detection time differences for QBER (single detections) and fidelity (double coincidence).

normal distribution with enough accuracy for the mechanism to provide the correct results. Then, the retrieved three center values for the three different frequencies are used in the system of equations of (5). The equation system has two independent variables, namely, Δf_k and t_{s_n}, one dependent variable θ_{q_k}, and three unknowns δf, θ'_q, and the systematic error in the time slot t_{s_n}. The three measurements with different, but known values of Δf_k allow solving this linear system of equations, as detailed in Section IV.

Fig. 5(a) presents the time histogram between time stamps for single qubit detections. Taking into account a time detection window of 80 time slots, the quantum nodes achieved a quantum bit error rate (QBER) better than 1% of the qubits transmitted, as shown in Fig. 5(b). Higher transmission rates, which required smaller detection time windows, led to increases in QBER. In addition, Fig. 5(a) shows the time-stamping histogram between pairs of qubits, for double

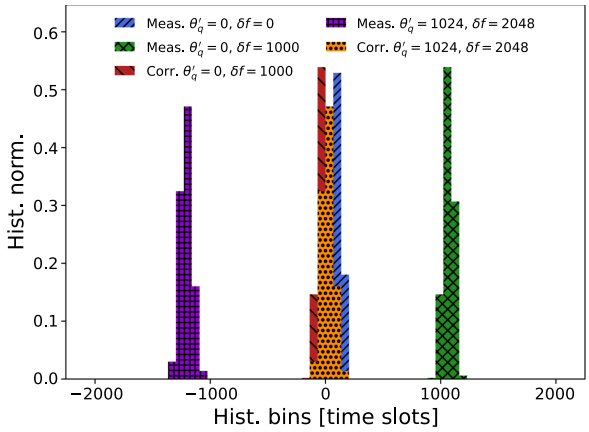

FIGURE 6. Histogram of the time offset measurements and corrections after applying the proposed mechanisms for three different cases of time and relative frequency offsets.

coincidence measurements. Accordingly, considering a coincidence time window of 140 time slots, an entanglement fidelity around 98% is achieved, as shown in Fig. 5(b), supporting the viability for multinode teleportation protocols. Further reducing the time window impacts on the achieved fidelity.

In general, the obtained histogram peaks follow a normal distribution as expected with the 24-MHz TCXO quartz-crystal clock with a temporal stability of 10^{-8} and 200-ns time jitter. Furthermore, at system space, the periodic correction every 100 ms provides an effective temporal stability better than 50 ns.

Correspondingly, Fig. 6 presents the effective temporal offset of the real-time clock with different phase θ'_q and relative frequency δf offsets. This allows one to evaluate different temporal conditions of the quantum link, such as different transmission times and relative frequency differences. Fig. 6 also presents the result of the time synchronization correction applying the temporal synchronization mechanism to different link conditions.

V. DISCUSSION OF RESULTS

The experimentally assembled system faithfully replicates the temporal alignment mechanism detailed in Section II. In particular, the experimental measurements presented in Section IV are replicable for all six links of the setup. To this extent, the capability to operate this mechanism in a multinode QN with different quantum link conditions is evidenced.

Accordingly, considering the same parameters for the mechanism as in Section IV, the temporal alignment correction error (ε) over $T_H = 4096$ time slots is measured for all combinations of links (e.g., Link AB stands for the channel connecting from node A to node B), as shown in Fig. 7(a). The value of 4096 time slots has been chosen for the experiments in Section IV to define the range of effective temporal offsets for the mechanism to be corrected. In particular, this value of 4096 is large enough to separate the different Δf_k given the present jitter, while it is still small enough so that

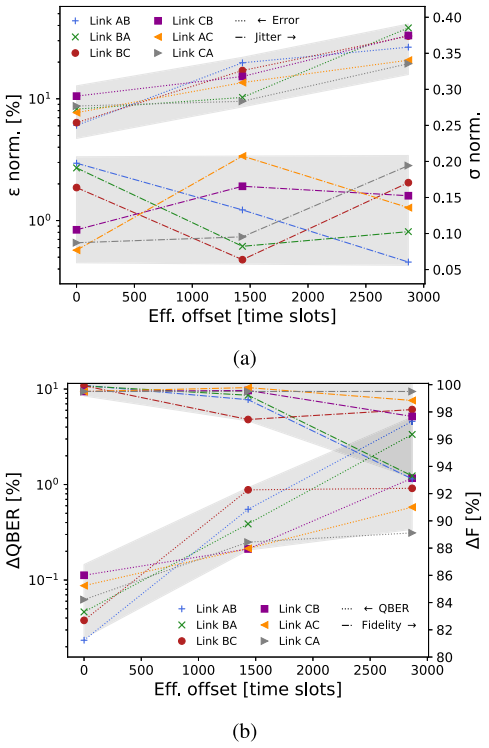

FIGURE 7. Results for six links between the three nodes. (a) Residual error and jitter of the temporal corrections, normalized to the time slot. (b) Impact of the residual errors and jitter to QBER and coincidence fidelity values.

the mechanism is sufficiently fast in order to execute and retrieve the synchronization parameters.

Correspondingly, the performance of the mechanism is characterized with ε, which is computed as the temporal absolute value of the center of the histogram distribution with respect to zero. Also, the jitter σ is one of the main contributors to the limits of the proposed mechanism [38]. Note that ε norm and σ norm in Fig. 7(a) are the error and jitter values divided by 4096, respectively. In particular, when the jitter is larger than the effective offset produced either by the initial offset or by the relative frequency difference, the mechanism will not correctly retrieve these values. However, in the latter situation, the temporal synchronization offset is already low enough for other synchronization algorithms implemented in the quantum protocols to fine-tune the synchronization to their needs.

In general, the residual time correction error is larger for larger equivalent effective temporal offsets, as expected. Notice that the different measurements for each link were performed one after the other, but with a time separation of 30 min, thus demonstrating long-time stability of the time stamping of the proposed system.

Furthermore, the mechanism is capable to operate with jitter, even when it is similar to the operational parameters of the mechanism. Also, as designed, the mechanism can operate in quantum links that have losses and, in general, high losses. The latter is of relevant importance for common

quantum protocols. Also, the suitability of the demonstrated mechanism to use the frequency parameter to test the temporal alignment of different links is remarkable, which entails no distortion with regard to the quantum state of transmitted qubits. Furthermore, the use of frequency testing allows both QNs operated with prepare-and-measure qubits as well as with triggered entangled qubits.

Moreover, from the results in Section IV, the assembled system in each ENBs has demonstrated the feasibility to connect the two space clocks, linking the real-time clock to the system clock at each node. Finally, the system clocks are all disciplined to the master PTP clock, which, in turn, are each adjusted with the proposed mechanism of this work, ensuring both short and long time stability.

Then, the results achieved in terms of temporal synchronization in a QN, with more than two nodes, are applied to analyze the performance that would be obtained in common quantum protocols. This analysis is theoretically extrapolated with respect to the performance baseline of the specific implementation of each quantum protocol. On the one hand, the reduction of performance in a communication quantum protocol, such as QKD, is studied in terms of the relevant QBER parameter. The QBER reduction is calculated as $\Delta\text{QBER} = \frac{1}{2}(1 - e^{-\varepsilon^2/(2\sigma^2 t_s)})$. The QBER reduction for different link conditions is shown in Fig. 7(b). Notice that the QBER reduction is below 10^{-1}, which is acceptable for most QKD use cases.

On the other hand, for quantum operation protocols, such as entanglement swapping between two nodes in teleportation protocols, where the quantum state of a third qubit is transferred, it is relevant to assess the double coincidence quantum fidelity. Accordingly, the reduction of fidelity with respect to its baseline value is computed as $\Delta\text{F} = e^{-\varepsilon^2/(2\sigma^2 t_s)}$. The fidelity decrease for different temporal alignment cases is shown in Fig. 7(b). The fidelity decrease still stays above 80% threshold value, which is required for most quantum teleportation protocols to operate.

The synchronization mechanism can be applied independently to each quantum link within the network. This means that synchronization is performed in a pairwise manner, which aligns well with the decentralized nature of QNs. Therefore, for each node L_N, synchronization procedures will be necessary, where L_N is the number of quantum links attached to the node. Each node will be allowed to execute this procedure in parallel for the L_N links, since for this work full-duplex quantum links are assumed. Then, for half-duplex quantum channels or quantum channels shared among more than two nodes, a more extended analysis should be performed (depending on the medium access control mechanisms implemented and quantum queue capabilities of the nodes), but in general terms, and as a first approximation, the synchronization mechanism proposed in this work scales as regular Telecom synchronization protocols.

Finally, with higher performance hardware clocks, the assembled experimental system could achieve larger than 100-MHz rate of qubits, making use of the proposed temporal alignment mechanism. Also, the time tagging resolution could be in the order of picoseconds making use of more precise time synchronization protocols, such as White Rabbit, and with dedicated hardware such as field-programmable gated array.

VI. CONCLUSION

Time-synchronized QNs are of great interest to exploit quantum resources and integration with current deployed telecommunication networks and infrastructure. In particular, aligning transmitted qubits in time is necessary and will address current challenges in the use of quantum protocols. Furthermore, this will open up to multinode QNs, rather than one-to-one quantum communications.

The proposed frequency testing quantum-state-preserving temporal alignment mechanism specifically addresses adjusting the common effective offsets in quantum links, leveraging mature regular telecommunication time synchronization protocols for enhanced robustness and performance. Furthermore, quantum computing algorithms and quantum synchronization protocols can be further applied to improve the performance of temporal synchronization in QNs.

This work can be extended to other types of time and spatial alignment for common quantum protocols. In this direction, further considerations can be addressed when accounting for future quantum memories, which will also help address dynamically changing QNs, as in the foreseen quantum internet.

ACKNOWLEDGMENT

The author acknowledges D. Rincón-Rivera, S. Sallent, and C. Cervelló-Pastor for fruitful discussions.

REFERENCES

[1] R. V. Meter, *Quantum Networking*, 1st ed.. Hoboken, NJ, USA: Wiley-ISTE, 2014, doi: 10.1002/9781118648919.

[2] J. I. Cirac, A. K. Ekert, S. F. Huelga, and C. Macchiavello, "Distributed quantum computation over noisy channels," *Phys. Rev. A*, vol. 59, no. 6, pp. 4249–4254, Jun. 1999, doi: 10.1103/PhysRevA.59.4249.

[3] D. Ferrari, S. Carretta, and M. Amoretti, "A modular quantum compilation framework for distributed quantum computing," *IEEE Trans. Quantum Eng.*, vol. 4, 2023, Art. no. 2500213, doi: 10.1109/TQE.2023.3303935.

[4] Y. Xia, Q. Zhuang, W. Clark, and Z. Zhang, "Entanglement-based distributed quantum sensing enhanced by quantum relays," in *Proc. Conf. Lasers Electro-Optics*, May 2019, pp. 1–2, doi: 10.1364/CLEO_QELS.2019.FTh4D.1.

[5] R. Camphausen et al., "Real-time entangled photon-pair imaging towards field deployment," *Proc. SPIE*, vol. 12795, Nov. 2023, Art. no. 1279502, doi: 10.1117/12.2691076.

[6] A. K. Ekert, "Quantum cryptography based on Bell's theorem," *Phys. Rev. Lett.*, vol. 67, no. 6, pp. 661–663, Aug. 1991, doi: 10.1103/PhysRevLett.67.661.

[7] C. H. Bennett and G. Brassard, "Quantum cryptography: Public key distribution and coin tossing," *Theor. Comput. Sci.*, vol. 560, pp. 7–11, Dec. 2014, doi: 10.1016/j.tcs.2014.05.025.

[8] M. Jofre et al., "Fast optical source for quantum key distribution based on semiconductor optical amplifiers," *Opt. Exp.*, vol. 19, no. 5, pp. 3825–3834, Feb. 2011, doi: 10.1364/OE.19.003825.

[9] S. Pironio et al., "Random numbers certified by Bell's theorem," *Nature*, vol. 464, no. 7291, pp. 1021–1024, Apr. 2010, doi: 10.1038/nature09008.

[10] M. Jofre et al., "True random numbers from amplified quantum vacuum," *Opt. Exp.*, vol. 19, no. 21, pp. 20665–20672, Oct. 2011, doi: 10.1364/OE.19.020665.

[11] T. Jennewein, U. Achleitner, G. Weihs, H. Weinfurter, and A. Zeilinger, "A fast and compact quantum random number generator," *Rev. Sci. Instrum.*, vol. 71, no. 4, pp. 1675–1680, Apr. 2000, doi: 10.1063/1.1150518.

[12] S. Lloyd, "Enhanced sensitivity of photodetection via quantum illumination," *Science*, vol. 321, no. 5895, pp. 1463–1465, Sep. 2008, doi: 10.1126/science.1160627.

[13] M. Malik, O. S. Magaña-Loaiza, and R. W. Boyd, "Quantum-secured imaging," *Appl. Phys. Lett.*, vol. 101, no. 24, Dec. 2012, Art. no. 241103, doi: 10.1063/1.4770298.

[14] C. Spiess et al., "Clock synchronization with correlated photons," *Phys. Rev. Appl.*, vol. 19, no. 5, May 2023, Art. no. 054082, doi: 10.1103/PhysRevApplied.19.054082.

[15] P. Zhang, N. Chen, S. Shen, S. Yu, S. Wu, and N. Kumar, "Future quantum communications and networking: A review and vision," *IEEE Wirel. Commun.*, vol. 31, no. 1, pp. 141–148, Feb. 2024, doi: 10.1109/MWC.012.2200295.

[16] N. Sangouard, C. Simon, H. d. Riedmatten, and N. Gisin, "Quantum repeaters based on atomic ensembles and linear optics," *Rev. Modern Phys.*, vol. 83, no. 1, pp. 33–80, Mar. 2011, doi: 10.1103/RevModPhys.83.33.

[17] H. Amellal, A. Meslouhi, Y. Hassouni, and M. E. Baz, "A quantum optical firewall based on simple quantum devices," *Quantum Inf. Process.*, vol. 14, no. 7, pp. 2617–2633, Jul. 2015, doi: 10.1007/s11128-015-1002-4.

[18] M. Afzelius, C. Simon, H. d. Riedmatten, and N. Gisin, "Multimode quantum memory based on atomic frequency combs," *Phys. Rev. A*, vol. 79, no. 5, May 2009, Art. no. 052329, doi: 10.1103/PhysRevA.79.052329.

[19] K. Bartkiewicz, A. Černoch, and K. Lemr, "Implementation of an efficient linear-optical quantum router," *Sci. Rep.*, vol. 8, no. 1, Sep. 2018, Art. no. 13480, doi: 10.1038/s41598-018-31273-0.

[20] N. Yu, C.-Y. Lai, and L. Zhou, "Protocols for packet quantum network intercommunication," *IEEE Trans. Quantum Eng.*, vol. 2, 2021, Art. no. 4103709, doi: 10.1109/TQE.2021.3112594.

[21] J. Illiano, M. Caleffi, A. Manzalini, and A. S. Cacciapuoti, "Quantum internet protocol stack: A comprehensive survey," *Comput. Netw.*, vol. 213, Aug. 2022, Art. no. 109092, doi: 10.1016/j.comnet.2022.109092.

[22] N. Gisin, G. Ribordy, W. Tittel, and H. Zbinden, "Quantum cryptography," *Rev. Modern Phys.*, vol. 74, no. 1, pp. 145–195, Mar. 2002, doi: 10.1103/RevModPhys.74.145.

[23] K. Heshami et al., "Quantum memories: Emerging applications and recent advances," *J. Modern Opt.*, vol. 63, no. 20, pp. 2005–2028, Nov. 2016, doi: 10.1080/09500340.2016.1148212.

[24] T. Gerrits et al., "Future time synchronization needs for quantum networks," Denver, CO, USA, 2022. [Online]. Available: https://wsts.atis.org/wp-content/uploads/2022/05/01-Thomas-Gerrits.Future-Time-Synchronization.pdf

[25] M. Alshowkan et al., "Advanced architectures for high-performance quantum networking," *J. Opt. Commun. Netw.*, vol. 14, no. 6, pp. 493–499, Jun. 2022, doi: 10.1364/JOCN.450201.

[26] S. F. Bush, W. A. Challener, and G. Mantelet, "A perspective on industrial quantum networks," *AVS Quantum Sci.*, vol. 3, no. 3, Aug. 2021, Art. no. 030501, doi: 10.1116/5.0051881.

[27] M. Alshowkan et al., "Synchronizing a quantum local area network with White Rabbit," in *Proc. Conf. Lasers Electro-Optics*, May 2022, Art. no. FM1C-4, doi: 10.1364/CLEO_QELS.2022.FM1C.4.

[28] T. Gerrits et al., "White Rabbit-assisted quantum network node synchronization with quantum channel coexistence," in *Proc. Conf. Lasers Electro-Optics*, May 2022, Art. no. FM1C-2, doi: 10.1364/CLEO_QELS.2022.FM1C.2.

[29] F. Granelli, R. Bassoli, J. Nötzel, F. H. P. Fitzek, H. Boche, and N. L. S. d. Fonseca, "A novel architecture for future classical-quantum communication networks," *Wirel. Commun. Mobile Comput.*, vol. 2022, Apr. 2022, Art. no. e3770994, doi: 10.1155/2022/3770994.

[30] D. Mills, "Internet time synchronization: The network time protocol," in *Proc. Internet Eng. Task Force, Request Comments RFC 1129*, Oct. 1989. [Online]. Available: https://datatracker.ietf.org/doc/rfc1129

[31] *IEEE Standard for a Precision Clock Synchronization Protocol for Networked Measurement and Control Systems*, IEEE Standard 1588-2002, 2002, doi: 10.1109/IEEESTD.2008.4579760.

[32] P. Moreira, J. Serrano, T. Wlostowski, P. Loschmidt, and G. Gaderer, "White Rabbit: Sub-nanosecond timing distribution over ethernet," in *Proc. Control Commun. Int. Symp. Precis. Clock Synchronization Meas.*, Oct. 2009, pp. 1–5, doi: 10.1109/ISPCS.2009.5340196.

[33] I. Marcikic, H. d. Riedmatten, W. Tittel, V. Scarani, H. Zbinden, and N. Gisin, "Time-bin entangled qubits for quantum communication created by femtosecond pulses," *Phys. Rev. A*, vol. 66, no. 6, Dec. 2002, Art. no. 062308, doi: 10.1103/PhysRevA.66.062308.

[34] B. Foundation, "BeagleBone black—Beagleboard documentation." Accessed: Jul. 9, 2024. [Online]. Available: https://docs.beagleboard.org/latest/boards/beaglebone/black/

[35] X. Zhao, D. M. Laverty, D. J. McKernan, K. McLaughlin, and S. Sezer, "GPS-Disciplined analog-to-digital converter for phasor measurement applications," *IEEE Trans. Instrum. Meas.*, vol. 66, no. 9, pp. 2349–2357, Sep. 2017, doi: 10.1109/TIM.2017.2700158.

[36] A. Libri, A. Bartolini, M. Magno, and L. Benini, "Evaluation of synchronization protocols for fine-grain HPC sensor data time-stamping and collection," in *Proc. Int. Conf. High Perform. Comput. Simul.*, Jul. 2016, pp. 818–825, doi: 10.1109/HPCSim.2016.7568419.

[37] Swabian Instruments, "Time tagger 20." Accessed: Jul. 9, 2024. [Online]. Available: https://www.swabianinstruments.com/time-tagger/

[38] P. J. Clarke et al., "Analysis of detector performance in a gigahertz clock rate quantum key distribution system," *New J. Phys.*, vol. 13, no. 7, Jul. 2011, Art. no. 075008, doi: 10.1088/1367-2630/13/7/075008.